Nano Research 2015, 8(9): 2842–2849
DOI 10.1007/s12274-015-0789-8
Research Article

ISSN 1998-0124
CN 11-5974/O4

High-quality-factor tantalum oxide nanomechanical resonators by laser oxidation of $TaSe_2$

Santiago J. Cartamil-Bueno[1] (✉), Peter G. Steeneken[1] (✉), Frans D. Tichelaar[2], Efren Navarro-Moratalla[3], Warner J. Venstra[1], Ronald van Leeuwen[1], Eugenio Coronado[3], Herre S.J. van der Zant[1], Gary A. Steele[1], and Andres Castellanos-Gomez[1,†] (✉)

[1] *Kavli Institute of Nanoscience, Delft University of Technology, Lorentzweg 1, 2628 CJ Delft, The Netherlands*
[2] *Kavli Institute of Nanoscience, Delft University of Technology, National Centre for HREM, Lorentzweg 1, 2628 CJ Delft, The Netherlands*
[3] *Instituto Ciencia Molecular (ICMol), Univ. Valencia, C/Catedrático José Beltrán 2, E-46980 Paterna, Spain*
[†] *Present address: Instituto Madrileño de Estudios Avanzados en Nanociencia (IMDEA-Nanociencia), 28049 Madrid, Spain*

Received: 10 December 2014
Revised: 7 April 2015
Accepted: 14 April 2015

KEYWORDS

$TaSe_2$,
tantalum oxide,
mechanical resonators,
laser oxidation,
optical interferometer,
high quality factor

ABSTRACT

Controlling the strain in two-dimensional (2D) materials is an interesting avenue to tailor the mechanical properties of nanoelectromechanical systems. Here, we demonstrate a technique to fabricate ultrathin tantalum oxide nanomechanical resonators with large stress by the laser oxidation of nano-drumhead resonators composed of tantalum diselenide ($TaSe_2$), a layered 2D material belonging to the metal dichalcogenides. Before the study of their mechanical properties with a laser interferometer, we verified the oxidation and crystallinity of the freely suspended tantalum oxide using high-resolution electron microscopy. We demonstrate that the stress of tantalum oxide resonators increases by 140 MPa (with respect to pristine $TaSe_2$ resonators), which causes an enhancement in the quality factor (14 times larger) and resonance frequency (9 times larger) of these resonators.

1 Introduction

Two-dimensional (2D) layered materials are attractive for high-frequency nanomechanical systems, which can be used in sensing applications. The reduced thickness and small mass of these materials enable high resonance frequencies f_0 and fast response times, whereas their low flexural rigidity increases the responsivity and allows size reduction. For low-noise operation of nanomechanical systems, it is desirable to achieve high quality factors Q at high frequencies. In conventional nanomechanical systems based on silicon nitride (Si_3N_4) beams, it has been shown that both f_0 and Q can be enhanced by increasing the stress

Address correspondence to Santiago J. Cartamil-Bueno, S.J.CartamilBueno@tudeflt.nl; Peter G. Steeneken, P.G.Steeneken@tudelft.nl; Andres Castellanos-Gomez, andres.castellanos@imdea.org

in the beam [1, 2]. Several methods have thus been proposed to tune the stress in nanomechanical systems based on 2D materials using temperature, mechanical actuators, and gas pressure [3–6]. For permanent stress modification in polycrystalline graphene, a method for direct bonding between graphene platelets has been proposed [6]. Because the mechanical properties of suspended crystalline 2D materials have attracted much attention for sensing applications, it is of scientific and technological interest to develop methods for local stress engineering in single-crystalline 2D materials.

In this work, we report a method that permanently modifies the stress in suspended single-crystalline 2D materials. We use a focused laser to locally increase the temperature of tantalum diselenide ($TaSe_2$) drumhead resonators until they undergo an oxidation process, which results in a drastic increase in the pre-stress of the selected 2D resonators. We investigated the effect of this increased pre-stress on the Q factor and resonance frequency, and observed a large enhancement for both properties in thin resonators (<20-nm thick). The pre-stress thereby provides a route toward higher f–Q products in layered material resonators. It was observed that the stress and thickness dependence of the Q factor are governed by the same model that was proposed to describe the Q factor of stressed Si_3N_4 beams [1, 2, 7].

2 Experimental

2.1 Fabrication of $TaSe_2$ drumhead resonators

$TaSe_2$ flakes were exfoliated from synthetic $TaSe_2$ crystals using mechanical exfoliation with blue Nitto tape (Nitto Denko Co., SPV 224P) [8]. More details can be found in Sections SI and SII in the Electronic Supplementary Material (ESM).

2.2 Laser oxidation of $TaSe_2$

A Renishaw inVia system was used to scan a focused laser spot (λ = 514 nm) over the $TaSe_2$ flakes. The oxidation of material was observed to occur at a power of 25 mW for 0.1–0.2 s of exposure time. The scanning step in the irradiation process was 300 nm.

2.3 Material characterization

Micro-Raman spectrometry and photoluminescence were used to characterize microregions of the materials, and a high-resolution electron microscope (Tecnai F20ST/STEM) with energy dispersive X-ray spectroscopy (EDX) detector allowed atomic resolution imaging and analysis of the elemental composition. See Sections SIV and SV in the ESM.

2.4 Mechanical resonance measurement

The frequency response of the drumhead resonators was determined using optical interferometry [9, 10]. We analyzed the fundamental mode, which is easily identified as it has the lowest frequency and highest intensity among all the mechanical resonance peaks in the spectrum. The measurement was performed in vacuum (~10^{-5} mbar) at room temperature. More information is available in Sections SVI and SIX in the ESM.

3 Results and discussion

For transmission electron microscopy (TEM) characterization, mechanically exfoliated $TaSe_2$ flakes were deposited onto a 200-nm Si_3N_4 membrane with holes (2.5 μm in diameter) using a recently developed dry transfer technique [11]. A focused green laser was scanned over part of the flakes to induce local laser oxidation in a confocal microscope system operated in air. Figure 1(a) presents a transmission mode optical image of the partially oxidized 50-nm-thick $TaSe_2$ flake. The regions labeled "1", "2", and "3" in Fig. 1(a) correspond to the pristine flake, laser-exposed flake, and bare Si_3N_4 membrane, respectively. A dramatic difference in the optical properties is observed between the pristine and laser-exposed areas of the flake even though the change in thickness of the laser-irradiated flakes was small (~3 nm), as observed in the atomic force microscopy (AFM) result, see Section SIII in the ESM. The optical transmittance of the suspended flake increased from 0.4 to 0.9 with the laser exposure, indicative of a reduced absorption coefficient of the material, as expected for tantalum oxide.

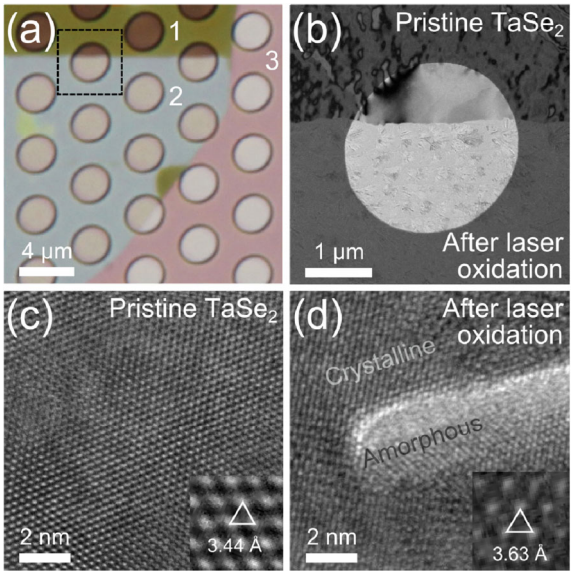

Figure 1 Characterization of a $TaSe_2$ flake before and after laser oxidation. (a) Transmission optical image showing pristine (1) and laser-oxidized (2) regions of the $TaSe_2$ flake on a silicon–nitride membrane TEM grid (3) with circular holes. (b) Bright-field TEM image of the partially oxidized suspended flake indicated by the dashed box in (a). (c) HRTEM image of suspended pristine $TaSe_2$. The interatomic distance (3.44 Å) corresponds to the Ta–Ta distance in the $\{1\bar{1}00\}$ plane of 2H–$TaSe_2$ [12]. (d) HRTEM image of a laser-oxidized region showing coexisting amorphous and crystalline phases. The interatomic distance in the hexagonal crystal plane increased to 3.63 Å.

To investigate the changes in the chemical composition caused by laser irradiation of $TaSe_2$ we performed EDX measurements on freely suspended areas of the material. Composition analysis revealed an approximate ratio of Ta/Se/O = 1.0/2.3/0.4 in the pristine flake. The presence of oxygen in the EDX results is attributed to surface oxidation of the $TaSe_2$ under atmospheric conditions (see Section SV in the ESM) [12]. Notably, after laser exposure, the composition of the flake was Ta/Se/O = 1.0/0.0/3.8, which indicates that the laser irradiation procedure in air oxidizes the flake, removing the selenium atoms and replacing them with oxygen. Thus, laser exposure converts the $TaSe_2$ into tantalum oxide. Note that this compositional analysis has an uncertainty of ±20%, hindering the determination of the exact stoichiometry after laser oxidation. Therefore, even though the O/Ta ratio determined by EDX was too large for Ta_2O_5, it was not possible to rule out that this tantalum oxide was Ta_2O_5 because of the uncertainties in EDX and the presence of surface oxides.

To determine the effect of laser oxidation on the crystal structure of the flake, we performed TEM analysis on the suspended flake. Figure 1(b) presents a bright-field TEM image of the region highlighted with a square in Fig. 1(a). The transition boundary between the pristine (top) and oxidized (bottom) part of the flake is abrupt (<50 nm). A high-resolution TEM (HRTEM) image of the pristine suspended $TaSe_2$ is shown in Fig. 1(c), demonstrating the hexagonal atomic configuration, which was confirmed by selective area diffraction pattern (SADP) analysis (see Section SV in the ESM). The crystal structure and lattice constant from HRTEM and SADP are consistent with an in-plane orientation of the layered $\{1\bar{1}00\}$ planes of 2H–$TaSe_2$ with an interatomic Ta–Ta spacing of 3.44 Å (inset). Figure 1(d) presents an HRTEM image of the oxidized region of the suspended material. Both amorphous and crystalline regions are observed. In the crystalline domains, the HRTEM image (inset) and SADP show a hexagonal configuration with an interatomic Ta–Ta spacing of 3.63 Å, which is larger than that in $TaSe_2$. The hexagonal structure and Ta–Ta distance obtained from TEM analysis of laser-oxidized $TaSe_2$ matches that of TT–Ta_2O_5 (also called δ–Ta_2O_5) [13–15]. Furthermore, the Raman spectrum and photoluminescence spectra (see Section SIV in the ESM) of the oxidized flake correspond to that of Ta_2O_5 [16]. These observations suggest that the modification is the oxidation reported in $TaSe_2$ when heated up to approximately T_{ox} = 600 ℃ [17], which results in a crystal structure that bears most resemblance to TT–Ta_2O_5.

The oxidation process in the suspended $TaSe_2$ occurs as follows. Once the temperature of $TaSe_2$ is increased above the critical temperature T_{ox} by laser heating, the material oxidizes and becomes more transparent. The increased transparency reduces light absorption and thus leads to a temperature reduction in the flake. Thus, despite inhomogeneities in the laser power and thermal resistances over the flake, this self-limiting mechanism prevents the flake from exposure to temperatures significantly higher than T_{ox}. This effect also prevents ablation [18] and improves the homogeneity of both the composition and stress in the oxidized film.

After establishing the effects of laser oxidation on

the composition and crystal structure of $TaSe_2$, we examined its effects on the mechanical properties of drumhead resonators. $TaSe_2$ drumhead resonators were fabricated by transferring mechanically exfoliated $TaSe_2$ flakes onto a SiO_2/Si substrate with circular cavities of 3.2 μm in diameter and 285 nm in depth. The mechanical properties of the drumhead resonators were investigated by measuring their fundamental mechanical resonance mode using an optical interferometer setup [9, 10] (see Section SVI in the ESM). The mechanical spectrum was measured over a wide frequency range, as shown in Section SIX, although we only used the fundamental mode for the analyses.

Figure 2 presents the mechanical resonance spectrum of a 17-nm-thick $TaSe_2$ drumhead resonator vibrating in its fundamental mode before and after laser oxidation. The insets show the corresponding optical images of the device and the square-shaped laser-exposed area containing the suspended drumhead in the oxidized case. The resonance frequency increases from f_{pris} = 10.2 MHz to f_{ox} = 39.6 MHz after oxidation, where f_{pris} and f_{ox} are the fundamental frequencies for the pristine and oxidized cases, respectively. At the same time, the Q factor increases from Q_{pris} = 357 to Q_{ox} = 1,058. A driven harmonic oscillator model fit the data and was used to determine the Q factor (solid lines). The magnitude of the interferometer signal after oxidation was a factor of 3,700 smaller than the signal before oxidation. This finding is attributed to a reduction of the photothermal actuation efficiency by the diminished optical absorption and to a reduction of the interferometric signal by reduction of the drum's reflectance after oxidation. After demonstrating the controlled enhancement of f_0 and Q, we proceeded to perform a systematic study on devices of different thickness.

Figure 3 shows the resonance frequencies and Q factors of 3.2-μm-diameter drums with thicknesses ranging from 6 to 89 nm, all from the same flake to ensure that they have the same built-in pre-stress, before (blue squares) and after laser oxidation (red circles). Starting with the pristine drums (blue data), for thick devices, we observed a linear relation between the resonance frequency and thickness because the bending rigidity dominates the mechanics of the resonator (the dashed lines represent this plate-like mechanical behavior). In the limit of small thickness, the resonance frequency converges to a constant value because the pre-stress dominates the mechanics (the dotted lines represent this membrane limit). In the oxidized drums (red circles in Fig. 3(a)), the resonance frequency behavior in the plate limit is similar to that of the pristine devices. However, the thin oxidized drums exhibit a much higher resonance frequency in the membrane limit, which indicates a larger pre-stress. The complete dataset is presented in Table S2 in Section SVII in the ESM.

To extract the stress increase caused by laser oxidation, we modeled the resonance frequency of the

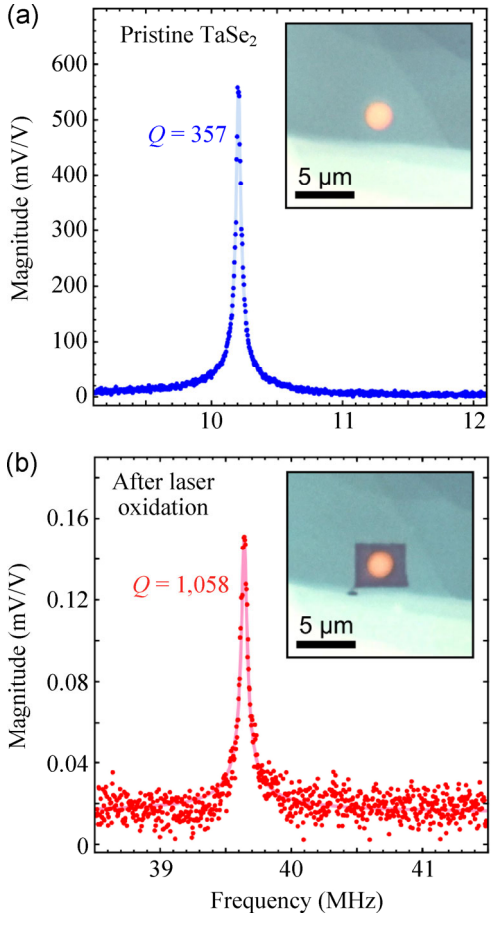

Figure 2 Mechanical resonances of $TaSe_2$ flakes before and after laser oxidation. (a) Fundamental mechanical resonance peak of a pristine 3.2-μm-diameter drum with a thickness of 17 nm. Inset: optical image of the drum. (b) Fundamental resonance peak of the same drum after laser oxidation of the square region shown in the inset. Large enhancements of the resonance frequency and Q factor are observed.

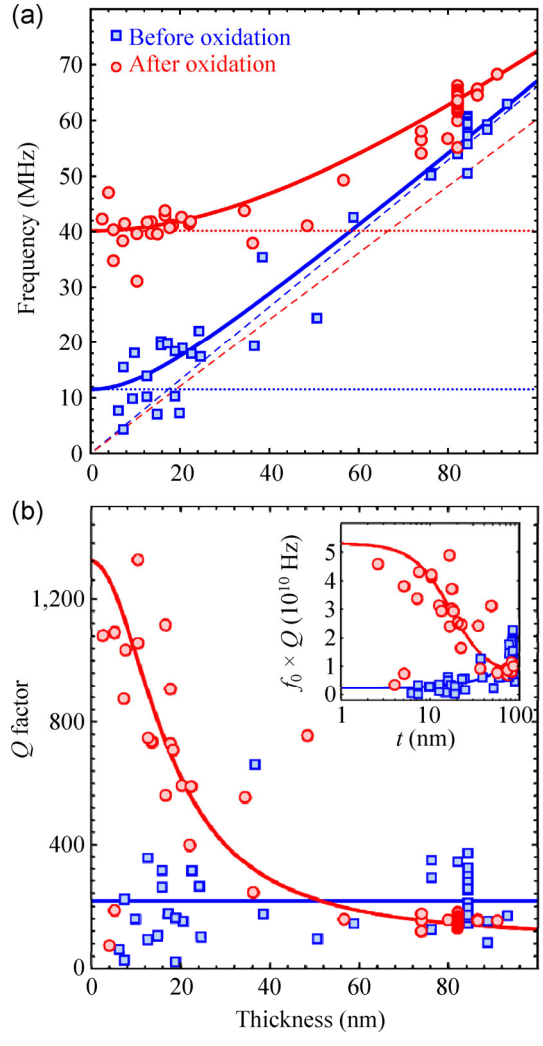

Figure 3 Thickness dependence of f_0 and Q of several drum resonators before and after laser oxidation. (a) Resonance frequency versus thickness of drums with a diameter of 3.2 μm from the same $TaSe_2$ flake before (blue squares) and after oxidation (red circles). Equation (2) (solid lines) is used to fit the data. For small thickness, the resonance frequency follows the membrane limit (horizontal dotted lines, Eq. (1)), whereas for thick drums, the data converges toward the plate limit (dashed lines, Eq. (1)). (b) Q factor versus thickness: For thin drums, an increase in Q is observed after laser oxidation. The solid red lines correspond to fits to the data using Eq. (3). Inset: In thin drums, laser oxidation increases the f–Q product.

drums as follows. For thin drums, the fundamental resonance frequency of the drums converges to the membrane limit f_{mem}, whereas for thick drums the frequency converges to the plate limit f_{plate} [19]

$$f_{mem} = \frac{2.40}{\pi d}\sqrt{\frac{\sigma}{\rho}} \quad f_{plate} = \frac{10.21}{\pi}\sqrt{\frac{E}{3\rho(1-\nu^2)}}\frac{t}{d^2} \qquad (1)$$

where E is Young's modulus, ν is Poisson's ratio ($\nu \approx 0.2$) [20], ρ is the mass density (ρ_{pris} = 8,660 kg/m^3, $\rho_{ox} = 0.655\rho_{pris}$ [17]), t is the thickness, d is the resonator diameter, and σ is the pre-stress in the drumhead. For drums of intermediate thickness, the resonance frequency can be approximated by the addition of the spring constants of the plate and membrane modes, giving

$$f_0 \approx \sqrt{f_{mem}^2 + f_{plate}^2} \qquad (2)$$

A fit of Eq. (2) to the data in Fig. 3(a) (solid lines) provides an estimate of E (E_{pris} = 110 GPa and E_{ox} = 60 GPa) and of the stress (σ_{pris} = 20 MPa and σ_{ox} = 160 MPa) values before and after oxidation. The estimated E for $TaSe_2$ is in good agreement with the values found in the literature [21–26]. Because the crystal structure of the oxidized flake consists of a mixture of amorphous and crystalline regions, it is not possible to compare the E of the oxidized flake and the data available in the literature. The fit shows a large increase of the tensile stress in the membrane from 20 to 160 MPa. The drastic increase in the resonance frequency during oxidation of the thin $TaSe_2$ drums can be mainly attributed to the increase in tensile stress.

Having clearly established the presence of oxidization-induced stress, we now address a possible mechanism for how this stress is created. The laser oxidation occurs locally and only heats up the material without significantly affecting the substrate beneath. During the recrystallization of the oxide at high temperature, T_{ox} = 600 ℃, atoms rearrange, which leads to stress relaxation in the suspended part of the drum. While cooling down, thermal contraction of the drum increases the stress in the membrane. An estimated value of the resulting tensile stress using the coefficient of thermal expansion $\alpha_{ox} = 3.6 \times 10^{-6}$ of Ta_2O_5 [27] yields $\sigma_{ox,e} \approx (T_{ox} - 25\ ℃)\alpha_{ox}E_{ox} = 120$ MPa, which is consistent with the measured stress σ_{ox} = 160 MPa.

In addition to changing the frequency of the mechanical resonators, the oxidization process also significantly changes the mechanical quality factor. Figure 3(b) shows the thickness dependence of the

quality factor of the fundamental resonance before and after laser oxidation. We find that the quality factor in pristine $TaSe_2$ resonators (blue squares) is almost independent of the thickness. For laser-oxidized drums, however, the quality factor shows strong thickness dependence: In thin oxidized drums, the quality factor is up to a factor of 9.4 higher than that in thick oxidized drums.

In the following part, we show that the increase of the Q factor originates from the large tensile stress of the thin oxidized drums. A similar increase in the Q factor in highly stressed thin membranes has been observed in Si_3N_4 resonators and reduced graphene oxide [2, 6, 7, 28–31]. The almost thickness-independent Q factor in low-stress (plate-like) drums observed in the pristine material can be phenomenologically described [6, 7] using a material model with a frequency-independent complex $E = E_1 + iE_2$. The imaginary part of E causes dissipation. Because the bending rigidity is proportional to E, the complex plate spring constant will be given by $k_{\text{plate}} = k_{\text{plate},1} + ik_{\text{plate},2}$. The Q factor of the resonator in the plate limit will therefore be given by $Q_{\text{plate}} = \frac{E_1}{E_2} = \frac{k_{\text{plate},1}}{k_{\text{plate},2}}$. Similarly, in the membrane limit, the Q factor can be expressed as $Q_{\text{mem}} = \frac{k_{\text{mem},1}}{k_{\text{mem},2}}$; however, because the losses resulting from elongation are much lower than the losses resulting from bending, we will assume that $Q_{\text{mem}} \gg Q_{\text{plate}}$ and $k_{\text{mem},2} \approx 0$. By adding the bending and membrane spring constants (as in Eq. (2)), the stress dependence of the Q factor is therefore given by $= \frac{k_{\text{mem},1} + k_{\text{plate},1}}{k_{\text{plate},2}}$. This relation indicates that a stress-induced increase of $k_{\text{mem},1}$ will result in an increase of the Q factor of the resonator.

Based on the relation $Q = \frac{k_{\text{mem},1} + k_{\text{plate},1}}{k_{\text{plate},2}}$, an equation for the Q ratio between pristine and oxidized drums is derived in Section SVIII in the ESM

$$\frac{Q_{\text{ox}}}{Q_{\text{pris}}} = \alpha \left(\frac{f_{\text{ox}}}{f_{\text{pris}}} \right)^2 \quad (3)$$

where the coefficient α is defined as $\alpha = \frac{m_{\text{ox}}}{m_{\text{pris}}} \frac{E_{2,\text{pris}}}{E_{2,\text{ox}}}$ and m is the mass of the drumhead. Equation (3) is used to fit the thickness dependence of Q_{ox} in Fig. 3(b) (solid lines). The values of f_{pris} and f_{ox} determined from the fits in Fig. 3(a) and an average value of Q_{pris} = 216 are used. By adjusting the coefficient $\alpha = 0.5$ as the only fit parameter, the thickness dependence of Q_{ox} is well captured by Eq. (3). The model based on a frequency-independent complex E, which was proposed to model the Q-factor increase with stress in Si_3N_4 beams [1, 7, 30, 32], is thus observed to be consistent with the thickness dependence of the Q factor in oxidized $TaSe_2$ flakes (Eq. (3)).

4 Conclusions

The f–Q product is an important figure of merit for micro- and nanoresonators, because high f–Q products can yield low-phase-noise high-frequency oscillators and sensors. Because tensile stress has been shown to increase both the resonance frequency and Q factor, the presented laser oxidation procedure is a very effective method to increase the f–Q product. The increase is as high as a factor of 42, yielding a maximum f–Q product of 4.9×10^{10} Hz. To our knowledge, the presented laser-oxidation method yields the highest f–Q product at room temperature in ultrathin resonators (t < 20 nm) composed of 2D materials, outperforming f–Q products reported in graphene and MoS_2 devices at room temperature [33].

In summary, a laser-oxidation procedure for the enhancement of the quality factor and resonance frequency of multilayer $TaSe_2$ resonators was presented. The procedure increases the stress in the drums by a factor of 8, because of thermal contraction during cooling after laser oxidation. The stress results in an enhanced resonance frequency (up to 9 times larger) and Q factor (over 14 times larger), which is attributed to a stress-induced increase in the spring constant. The presented laser oxidation procedure thus provides a tool for the selective local modification of the mechanical properties of 2D materials. This ability enables interesting applications, such as *in-situ* tuning of the resonance frequency and Q factor, and the

engineering of mechanical mode shapes and intermode relations by the selective patterning of stress regions in suspended flakes (see Sections SIX and SX in the ESM). The same procedure is expected to be applicable to other 2D materials, as many metal dichalcogenides show oxidation reactions similar to $TaSe_2$ [17, 34].

Acknowledgements

The research leading to these results has received funding from the European Union Seventh Framework Programme under grant agreement no 604391 Graphene Flagship. W. J. V. acknowledges financial support through NanoNextNL, a micro and nanotechnology consortium of the Netherlands and 130 partners, and the European Union's Seventh Framework Programme (FP7) under Grant Agreement no. 318287, project LANDAUER. A. C. G. acknowledges financial support through the FP7-Marie Curie Projects PIEFGA-2011-300802 ("STRENGTHNANO").

Electronic Supplementary Material: Supplementary material (the synthesization of $TaSe_2$, the fabrication and laser-oxidation of resonators; AFM, Raman, PL, and TEM characterizations; an explanation of the optical interferometer setup, the complete datasets, the model for stress-dependent Q factor, a wide frequency spectra of pristine and oxidized resonators, and an application of the local oxidation of resonators) is available in the online version of this article at http://dx.doi.org/10.1007/s12274-015-0789-8.

References

[1] Adiga, V. P.; Ilic, B.; Barton, R. A.; Wilson-Rae, I.; Craighead, H. G.; Parpia, J. M. Modal dependence of dissipation in silicon nitride drum resonators. *Appl. Phys. Lett.* **2011**, *99*, 253103.

[2] Wilson-Rae, I.; Barton, R. A.; Verbridge, S. S.; Southworth, D. R.; Ilic, B.; Craighead, H. G.; Parpia, J. M. High-Q nanomechanics via destructive interference of elastic waves. *Phys. Rev. Lett.* **2011**, *106*, 047205.

[3] Singh, V.; Sengupta, S.; Solanki, H. S.; Dhall, R.; Allain, A.; Dhara, S.; Pant, P.; Deshmukh, M. M. Probing thermal expansion of graphene and modal dispersion at low-temperature using graphene nanoelectromechanical systems resonators. *Nanotechnology* **2010**, *21*, 165204.

[4] Koenig, S. P.; Wang, L. D.; Pellegrino, J.; Bunch, J. S. Selective molecular sieving through porous graphene. *Nat. Nanotechnol.* **2012**, *7*, 728–732.

[5] Pérez Garza, H. H.; Kievit, E. W.; Schneider, G. F.; Staufer, U. Controlled, reversible, and nondestructive generation of uniaxial extreme strains (>10%) in graphene. *Nano Lett.* **2014**, *14*, 4107–4113.

[6] Zalalutdinov, M. K.; Robinson, J. T.; Junkermeier, C. E.; Culbertson, J. C.; Reinecke, T. L.; Stine, R.; Sheehan, P. E.; Houston, B. H.; Snow, E. S. Engineering graphene mechanical systems. *Nano Lett.* **2012**, *12*, 4212–4218.

[7] Unterreithmeier, Q. P.; Faust, T.; Kotthaus, J. P. Damping of nanomechanical resonators. *Phys. Rev. Lett.* **2010**, *105*, 027205.

[8] Castellanos-Gomez, A.; Navarro-Moratalla, E.; Mokry, G.; Quereda, J.; Pinilla-Cienfuegos, E.; Agraït, N.; van der Zant, H. S. J.; Coronado, E.; Steele, G. A.; Rubio-Bollinger, G. Fast and reliable identification of atomically thin layers of $TaSe_2$ crystals. *Nano Res.* **2013**, *6*, 191–199.

[9] Castellanos-Gomez, A.; van Leeuwen, R.; Buscema, M.; van der Zant, H. S. J.; Steele, G. A.; Venstra, W. J. Single-layer MoS_2 mechanical resonators. *Adv. Mater.* **2013**, *25*, 6719–6723.

[10] Bunch, J. S.; van der Zande, A. M.; Verbridge, S. S.; Frank, I. W.; Tanenbaum, D. M.; Parpia, J. M.; Craighead, H. G.; McEuen, P. L. Electromechanical resonators from graphene sheets. *Science* **2007**, *315*, 490–493.

[11] Castellanos-Gomez, A.; Buscema, M.; Molenaar, R.; Singh, V.; Janssen, L.; van der Zant, H. S. J.; Steele, G. A. Deterministic transfer of two-dimensional materials by all-dry viscoelastic stamping. *2D Mater.* **2014**, *1*, 011002.

[12] Yan, Z.; Jiang, C.; Pope, T. R.; Tsang, C. F.; Stickney, J. L.; Goli, P.; Renteria, J.; Salguero, T. T.; Balandin, A. A. Phonon and thermal properties of exfoliated $TaSe_2$ thin films. *J. Appl. Phys.* **2013**, *114*, 204301.

[13] Hummel, H.-U.; Fackler, R.; Remmert, P. Tantaloxide durch gasphasenhydrolyse, druckhydrolyse und transportreaktion aus 2H-TaS_2: Synthesen von $TTTa_2O_5$ und TTa_2O_5 und kristallstruktur von TTa_2O_5. *Chem. Ber.* **1992**, 551–556.

[14] Terao, N. Structure des oxides de tantale. *Jpn. J. Appl. Phys.* **1967**, *6*, 21.

[15] Moser, R. Single-crystal growth and polymorphy of Nb_2O_5 and Ta_2O_5. *Schweiz. Mineral. Petrogr. Mitt.* **1965**, *45*, 38–101.

[16] Dobal, P. S.; Katiyar, R. S.; Jiang, Y.; Guo, R.; Bhalla, A. S. Raman scattering study of a phase transition in tantalum pentoxide. *J. Raman Spectrosc.* **2000**, *31*, 1061–1065.

[17] Lavik, M. T.; Medved, T. M.; Moore, G. D. Oxidation characteristics of MoS_2 and other solid lubricants. *ASLE Trans.* **1968**, *11*, 44–55.

[18] Castellanos-Gomez, A.; Barkelid, M.; Goossens, A. M.; Calado, V. E.; van der Zant, H. S. J.; Steele, G. A. Laser-thinning of MoS_2: On demand generation of a single-layer semiconductor. *Nano Lett.* **2012**, *12*, 3187–3192.

[19] Wah, T. Vibration of circular plates. *J. Acoust. Soc. Am.* **1962**, *34*, 275–281.

[20] Kang, J.; Tongay, S.; Zhou, J.; Li, J. B.; Wu, J. Q. Band offsets and heterostructures of two-dimensional semiconductors. *Appl. Phys. Lett.* **2013**, *102*, 012111.

[21] Barmatz, M. Elastic measurements in one and two-dimensional compounds. *Ultrason. Symp. Proc.* **1974**, *1–3*, 461–467.

[22] Barmatz, M.; Testardi, L. R.; Di Salvo, F. J. Elasticity measurements in the layered dichalcogenides $TaSe_2$ and $NbSe_2$. *Phys. Rev. B* **1975**, *12*, 4367.

[23] Chu, C. W.; Testardi, L. R.; Di Salvo, F. J.; Moncton, D. E. Pressure effects on the charge-density-wave phases in 2 H-$TaSe_2$. *Phys. Rev. B* **1976**, *14*, 464.

[24] Feldman, J. L.; Vold, C. L.; Skelton, E. F.; Yu, S. C.; Spain, I. L. X-ray diffraction studies and thermal and elastic properties of 2 H-$TaSe_2$. *Phys. Rev. B* **1978**, *18*, 5820.

[25] Abdullaev, N. A. Elastic properties of layered crystals. *Phys. Solid State* **2006**, *48*, 663–669.

[26] Dub, S. N.; Starikov, V. V. Elasticity module and hardness of niobium and tantalum anode oxide films. *Funct. Mater.* **2007**, *14*, 347–350.

[27] Tien, C.-L.; Lee, C.-C.; Chuang, K.-P.; Jaing, C.-C. Simultaneous determination of the thermal expansion coefficient and the elastic modulus of Ta_2O_5 thin film using phase shifting interferometry. *J. Mod. Opt.* **2000**, *47*, 1681–1691.

[28] Schmid, S.; Jensen, K. D.; Nielsen, K. H.; Boisen, A. Damping mechanisms in high-Q micro and nanomechanical string resonators. *Phys. Rev. B* **2011**, *84*, 165307.

[29] Yu, P.-L.; Purdy, T. P.; Regal, C. A. Control of material damping in high-Q membrane microresonators. *Phys. Rev. Lett.* **2012**, *108*, 083603.

[30] Adiga, V. P.; Ilic, B.; Barton, R. A.; Wilson-Rae, I.; Craighead, H. G.; Parpia, J. M. Approaching intrinsic performance in ultra-thin silicon nitride drum resonators. *J. Appl. Phys.* **2012**, *112*, 064323.

[31] Kermany, A. R.; Brawley, G.; Mishra, N.; Sheridan, E.; Bowen, W. P.; Iacopi, F. Microresonators with Q-factors over a million from highly stressed epitaxial silicon carbide on silicon. *Appl. Phys. Lett.* **2014**, *104*, 081901.

[32] Lee, S.; Adiga, V. P.; Barton, R. A.; van der Zande, A. M.; Lee, G.-H.; Ilic, B. R.; Gondarenko, A.; Parpia, J. M.; Craighead, H. G.; Hone, J. Graphene metallization of high-stress silicon nitride resonators for electrical integration. *Nano Lett.* **2013**, *13*, 4275–4279.

[33] Lee, J.; Wang, Z. H.; He, K. L.; Shan, J.; Feng, P. X.-L. High frequency MoS_2 nanomechanical resonators. *ACS Nano* **2013**, *7*, 6086–6091.

[34] Coronado, E.; Forment-Aliaga, A.; Navarro-Moratalla, E.; Pinilla-Cienfuegos, E.; Castellanos-Gomez, A. Nanofabrication of TaS_2 conducting layers nanopatterned with Ta_2O_5 insulating regions via AFM. *J. Mater. Chem. C* **2013**, *1*, 7692–7694.